ADVANCES IN ATMOSPHERIC SCIENCES, VOL. 31, JULY 2014, 851–862

Planetary Wave Reflection and Its Impact on Tropospheric Cold Weather over Asia during January 2008

Debashis NATH, CHEN Wen*, WANG Lin, and MA Yin

Center for Monsoon System Research, Institute of Atmospheric Physics, Chinese Academy of Sciences, Beijing 100190

(Received 25 September 2013; revised 06 December 2013; accepted 19 December 2013)

ABSTRACT

Reflection of stratospheric planetary waves and its impact on tropospheric cold weather over Asia during January 2008 were investigated by applying two dimensional Eliassen–Palm (EP) flux and three-dimensional Plumb wave activity fluxes. The planetary wave propagation can clearly be seen in the longitude–height and latitude–height sections of the Plumb wave activity flux and EP flux, respectively, when the stratospheric basic state is partially reflective. Primarily, a wave packet emanating from Baffin Island/coast of Labrador propagated eastward, equatorward and was reflected over Central Eurasia and parts of China, which in turn triggered the advection of cold wind from the northern part of the boreal forest regions and Siberia to the subtropics. The wide region of Central Eurasia and China experienced extreme cold weather during the second ten days of January 2008, whereas the extraordinary persistence of the event might have occurred due to an anomalous blocking high in the Urals–Siberia region.

Key words: planetary wave reflection, reflective index, advection, blocking, cold weather

Citation: Nath, D., W. Chen, L. Wang, and Y. Ma, 2014: Planetary wave reflection and its impact on tropospheric cold weather over Asia during January 2008. *Adv. Atmos. Sci.*, **31**(4), 851–862, doi: 10.1007/s00376-013-3195-8.

1. Introduction

In the Northern Hemisphere winter, the stratospheric and tropospheric circulations are dynamically coupled through the upward propagation of planetary waves (Chen and Huang, 2002, Lan et al., 2012). In the last few decades, many studies have revealed the impact of stratospheric dynamic processes on tropospheric climate variability through the downward coupling between the stratosphere and troposphere. Hines (1974) and Geller and Alpert (1980) proposed the possibility of planetary wave reflection in the light of stratosphere–troposphere coupling (STC). In the recent era, the subject of reflection and its impact on the tropospheric field has become more and more interesting. Several studies have demonstrated the downward propagation of anomalous zonal mean zonal winds (Kodera et al., 1990; Kuroda and Kodera, 1999; Christiansen, 2000; Chen and Li, 2007), STC processes in relation to the Northern Annular modes (NAM; Baldwin and Dunkerton, 1999; Baldwin and Dunkerton, 2001; Deng et al., 2008; Li et al., 2012; Chen et al., 2013), and downward propagation of stratospheric signature due to strong wave–mean-flow interaction (Baldwin and Dunkerton, 2001; Christiansen, 2001; Chen and Wei, 2009; Nath et al., 2013).

Holton and Mass (1976) and Kodera et al. (2000) discussed the shifts in the region of strongest interaction between the upward propagating Rossby waves and stratospheric zonal flow, which may result in a poleward and downward progression of the mean flow perturbations (Perlwitz and Harnik, 2004) (hereafter PH04). Due to the gradual increase in the air density downward, the impact of the reflected component of planetary waves on the troposphere is considered to be small; however, the recent statistical works by Perlwitz and Graf (2001), Perlwitz and Harnik (2003) (hereafter PH03) and PH04 discussed the downward coupling processes of zonal wavenumber 1 (WN1) and zonal wavenumber 2 (WN2) in the light of stratospheric dynamical states. They statistically categorized the stratospheric winter states into reflective and nonreflective states, using lagged correlation analysis. In general the reflective and nonreflective states correspond to stronger and weaker polar vortices, respectively, e.g., there exists downward propagation of stratospheric anomalies after sudden stratospheric warming events, the definition in PH03 is different from the conventional concept of downward propagation of upper stratospheric anomalies to the middle and lower stratosphere. During the reflective background state, they found the dominance of WN1 and the zonal mean component in the shorter ($\sim$ 12 days) and longer time scales, respectively. They also observed a westward and eastward phase tilt of the WN1 regression patterns (leading mode) with increasing altitude for negative and positive time lags, respectively, and the features were consistent with the downward reflection of the planetary waves.

In recent years, several studies have emphasized the STC

* Corresponding author: CHEN Wen
Email: cw@post.iap.ac.cn

processes in the light of annular modes and the strength of the polar vortex (Baldwin and Dunkerton, 1999; Kuroda and Kodera, 1999; Baldwin and Dunkerton, 2001; Christiansen, 2001; Chen et al., 2002). Large geopotential anomalies propagate down to the troposphere and are followed by an anomalous change in weather and circulation patterns, bearing a close resemblance to the features of the NAM. During nonreflective years, the signature of NAM anomalies is quite prominent on the surface, whereas during the reflective winters the signal gets attenuated well above the tropopause (PH04). Statistically, the coupling between the stratospheric and tropospheric NAM-like anomalies are stronger during weak polar vortex years (Baldwin and Dunkerton, 1999; Baldwin and Dunkerton, 2001); whereas, the signature of WN1 reflection is more prominent during strong polar vortex years (Perlwitz and Graf, 2001). However, Kodera et al. (2000) discussed the intraseasonal variability in the coupling processes with maximum and minimum occurrences during late-winter–spring and fall–early-winter, respectively.

Coughlin and Tung (2005) and Kodera et al. (2008) observed the reflection of planetary waves in conjunction with major stratospheric warming (SSW) and discussed the impact on tropospheric weather regimes. Coughlin and Tung (2005) reported the change in the WN1 field in the troposphere due to the reflection of planetary waves in the stratosphere, whereas Kodera et al. (2008) considered the total wavenumber field to demonstrate the reflection of planetary waves during the sudden stratospheric warming of March 2007, in which the upward propagating waves from continental Eurasia were reflected back to the North American sector, resulting in very cold weather over the northeast coast of the North American continent. Kodera and Chiba (1995) investigated the impact of the stratosphere on the tropospheric circulation patterns during an SSW event in 1984–85 through the meridional propagation of planetary waves. Although several mechanisms were proposed, the transmission of zonal mean perturbations to the troposphere during the winter months are still not well understood.

In the present study, we found a special case prior to the major stratospheric warming of January 2008, in which the waves propagated upward and eastward from Baffin Island and the coast of Labrador and reflected back to continental western Eurasia and South-central Russia and China. As reported earlier, there was an anomalously strong East Asian winter monsoon in January 2008, with record-breaking and persistent cold events, snowfall and freezing rain over West Asia and South-central China (Zhou et al., 2009). This extreme event caused excessive damage and disruption over South China, and led to a huge number of broken power transmission lines and chaotic traffic conditions. The disaster incurred a loss of 53.8 billion RMB (Zhou et al., 2009). The event was closely related to anomalous northerlies from the Arabian Peninsula and was induced by a preceding cold surge from West Asia around 16 January 2008 (Wang et al., 2012). The 2008 event was the coldest event for at least the period 1979–2008. Most studies have concentrated on explaining the abnormal cold weather over China. Zhou et al. (2009) and Hui (2009) identified the key factors as the blocking high over Siberia, strong persistent southwesterly flow, a deep inversion layer in the lower troposphere, and abnormal circulations at high latitudes. Hui (2009) showed that, during January 2008, the northern polar vortex index from 850 to 100 hPa was negative and hence the polar vortex was stronger, which was favorable for the reflection of planetary waves. Wen et al. (2009) reported strong precursory signals of the variability of January temperature in the light of Arctic Oscillation (AO) and the Middle East Jet Stream. They showed that the AO value was 0.82 in January 2008, and linked the positive AO index to the increase in temperature over China. Some studies have also discussed the roles of stratospheric circulation (Wang et al., 2009; Chen et al., 2009). In a separate study, Wang et al. (2012) demonstrated the triggering of Madden–Julian Oscillation in late January 2008 by a cold surge over West Asia. However, none of the studies mentioned above clearly demonstrate the exact mechanism of the extreme event.

The present study attempts to demonstrate a clear connection between planetary wave reflection and the occurrence of cold events in January 2008. Section 2 deals with the data and methodology of the analysis. The main results are reported and discussed in section 3. Concluding remarks are given in section 4.

2. Data and methodology

2.1. *Data*

This study is mainly based on the daily reanalysis data from the European Centre for Medium-Range Weather Forecasts (ECMWF) Re-Analysis Interim dataset (ERA-Interim; Uppala et al., 2008; Dee et al., 2011). We used the ERA-Interim products for geopotential height (H), zonal wind (U), meridional wind (V), temperature (T) and potential vorticity (PV) data. We also used the National Centers for Environmental Prediction–National Center for Atmospheric Research (NCEP–NCAR) CDAS-1 daily streamfunction (psi) data from the International Research institute for Climate and Society, Columbia (http://iridl.ldeo.columbia.edu/expert/SOURCES/.NOAA/.NCEP-NCAR/.CDAS-1/.MONTHLY/.Intrinsic/.PressureLevel/.psi). We used these daily mean data for the period from December 2007 to April 2008. The data are available for 37 and 17 pressure levels from 1000 to 1 hPa and 1000 to 10 hPa, with horizontal resolutions of $1.5^\circ \times 1.5^\circ$ and $2.5^\circ \times 2.5^\circ$ for ECMWF and NCEP–NCAR, respectively.

2.2. *Methodology*

2.2.1. *The reflective index*

PH04 categorized the reflective and nonreflective basic states for planetary wave reflection based on the zonal mean zonal wind difference between 2 and 10 hPa, averaged over 58°–74°N and over time. They defined the reflective index as

$$U_{\rm ri} = \bar{U}_2 - \bar{U}_{10}. \quad (1)$$

Positive and negative index values correspond to nonreflective and reflective basic states, respectively. Although PH04 defined the reflective index for the temporal and zonal mean zonal wind field, in the present study we are more interested in qualitatively understanding the longitudinal and daily variability of the reflecting structure in the midstratosphere.

2.2.2. *The Eliassen–Palm flux*

In the meridional plane, the Eliassen–Palm (EP) flux indicates the quasigeostropic eddy forcing of the zonal mean planetary wave propagation (Andrews et al., 1987; Holton, 2004). Usually, EP fluxes are displayed in the form of vectors for representing the direction of wave propagation, which have the components along the meridional (F_y) and vertical (F_z) planes

$$F_y = -\rho r \cos\theta \overline{u'v'} \quad \text{(Momentum flux)}, \tag{2}$$

$$F_z = \rho f R r \cos\theta \overline{v'T'}/(N^2 H_s) \quad \text{(Heat flux)}, \tag{3}$$

where ρ, R, u', v', and T' are the air density, gas constant, zonal, meridional and temperature perturbations, respectively, and the overbars indicate zonal average. N^2 and H_s represent the squared Brunt Vaisala frequency and the scale height. For better representation, the EP fluxes are scaled by the inverse of air density. The eddies exert a zonal force by accelerating and decelerating the westerly zonal flow and can be measured from the divergence and convergence of EP fluxes, respectively (e.g., Harada et al., 2010; Li et al., 2011). In the present study, we calculated the EP flux for the eddy field, i.e., the deviation from the zonal mean field.

2.2.3. *The Plumb three dimensional wave activity flux (Plumb flux)*

Although the EP flux gives an impression of meridional propagation, planetary waves can also propagate zonally (Hayashi, 1981). Hence, Plumb (1985) introduced the concept of wave propagation from the troposphere to the stratosphere in three-dimensional space. In the log-pressure coordinates the wave activity flux F_s can be represented as follows:

$$F_s = p\cos\theta \begin{pmatrix} \frac{1}{2r^2\cos^2\theta}\left[\left(\frac{\partial\psi'}{\partial\lambda}\right)^2 - \psi'\frac{\partial^2\psi'}{\partial\lambda^2}\right] \\ \frac{1}{2r^2\cos\theta}\left[\frac{\partial\psi'}{\partial\lambda}\frac{\partial\psi'}{\partial\theta} - \psi'\frac{\partial^2\psi'}{\partial\lambda\partial\theta}\right] \\ \frac{2\Omega^2\sin^2\theta}{N^2 r\cos\theta}\left[\frac{\partial\psi'\partial\psi'}{\partial\lambda\partial z} - \psi'\frac{\partial^2\psi'}{\partial\lambda\partial z}\right] \end{pmatrix}, \tag{4}$$

where ψ, λ, Ω, z are the streamfunction, longitude, Earth's rotation rate, altitude, respectively, and $p =$ pressure/1000 hPa. The primes in the equation represent the perturbation fields. Kodera et al. (2008) and Harada et al. (2010) considered daily and three-day mean snapshots of the stationary wave activity fluxes to address the upward propagation of the wave packets from Eurasia and Alaska during 2007 and 2009 sudden stratospheric warming events, respectively. We calculated the Plumb flux for the eddy field, i.e., the deviation from the zonal mean field.

2.2.4. *Blocking index*

Atmospheric blocking is associated with the blocking of the midlatitude westerly jet and the formation of anomalous local easterly flow and is characterized by an appreciable mass difference between high- and midlatitudes (Namias and Clapp, 1951; Treidl et al., 1981; Barriopedro et al., 2006). Usually, the blocking patterns are quasi-stationary and can persist for a week (Ural blocking) to 2–3 weeks, or even longer (North Atlantic blocking), leading to a significant redistribution of rainfall and the occurrence of an extreme drought season. The blocking also produces a strong southward advection of the polar air, inducing extremely cold weather in winter months. Zhou et al. (2009) reported the occurrences of an extraordinary persistent blocking high over the Urals–Siberia region during January 2008. The blocking frequency exceeded the climatological high in the longitudinal band of 55°–70°E. We have computed the blocking index from Tibaldi and Molteni (1990), with the additional criteria proposed by Barriopedro et al. (2006). The 500-hPa geopotential height gradients (GHGN and GHGS) were simultaneously computed using the following expressions:

$$\text{GHGN} = \frac{H(\lambda,\theta_N) - H(\lambda,\theta_0)}{\theta_N - \theta_0}, \tag{5a}$$

$$\text{GHGN} = \frac{H(\lambda,\theta_0) - H(\lambda,\theta_S)}{\theta_0 - \theta_N}, \tag{5b}$$

where $H(\lambda,\theta)$ is the 500-hPa geopotential height, GHGS is the measure of zonal geostrophic wind component, and GHGN is imposed to exclude the nonblocked flows (Barriopedro et al., 2006). θ_N, θ_S and θ_0 are the latitudes, where, $\theta_N = 78.0 + \delta, \theta_0 = 60.0 + \delta, \theta_S = 39.5 + \delta, \delta = -4.5, -3.0, -1.5, 0.0, 1.5, 3.0, 4.5$. An arbitrary longitude is considered to be blocked if the following conditions are satisfied: GHGN < -10, GHGS > 0, $Z(\lambda,\theta_0) - \overline{Z(\lambda,\theta_0)} > 0$. To identify the potential blocks, a three-day running mean filter was applied at each longitude.

2.2.5. *Thermal advection*

We calculated the thermal advection using the following equation:

$$\left(\frac{\partial T}{\partial t}\right)_{\text{adv}} = -\left(U\frac{\partial T}{\partial x} + V\frac{\partial T}{\partial y}\right), \tag{6}$$

where $U, V, T, \partial T/\partial t, \partial T/\partial x$ and $\partial T/\partial y$ are the zonal wind, meridional wind, temperature, time derivative of temperature, and thermal gradient along zonal and meridional directions, respectively.

3. Results and discussion

3.1. *Stratospheric reflective state and two dimensional wave propagation*

PH04 categorized the reflecting and nonreflecting basic states based on the index shown in Eq. (1). Unlike the zonal and time averages, we have plotted the time–longitude sec-

tion of the reflective index in Fig. 1, to obtain the zonal distribution of the reflective index pattern as a function of time. In addition to PH04, we calculated the index based on the zonal mean zonal wind difference between 10 and 50 hPa (hereafter Uri2), averaged over 58°–74°N (lower panel), as well using the conventional approach (hereafter Uri1) as in Eq. (1) (upper panel). The index is not always zonally-symmetric; rather, it is negative over the North Atlantic Ocean and east of Eurasia, i.e., the polar night jet peaks in the midstratosphere and is positive over West Eurasia for Uri1 (upper panel). The pattern propagates farther eastward as a function of time and height (Uri2) until 21 January, and thereafter a high negative index persists throughout the longitude until the end of the month. This prompts us to conclude that the basic state is partially reflective during the event, and in such cases the zonal mean may not be a true diagnostic to characterize the reflective and nonreflective stratospheric states. The eastward tilt in the reflective index pattern is more favorable to guide the waves downward and eastward of the source region.

Figure 2 shows the daily march of EP flux vectors, overplotted with zonal mean zonal wind during 10–21 January 2008. The EP flux vectors are parallel to the local group velocity and its convergence indicated the retardation of the zonal flow due to wave forcing (Kodera et al., 2008). However, to address the issue of wave reflection, EP flux vectors alone may not be sufficient; hence, we have also plotted the

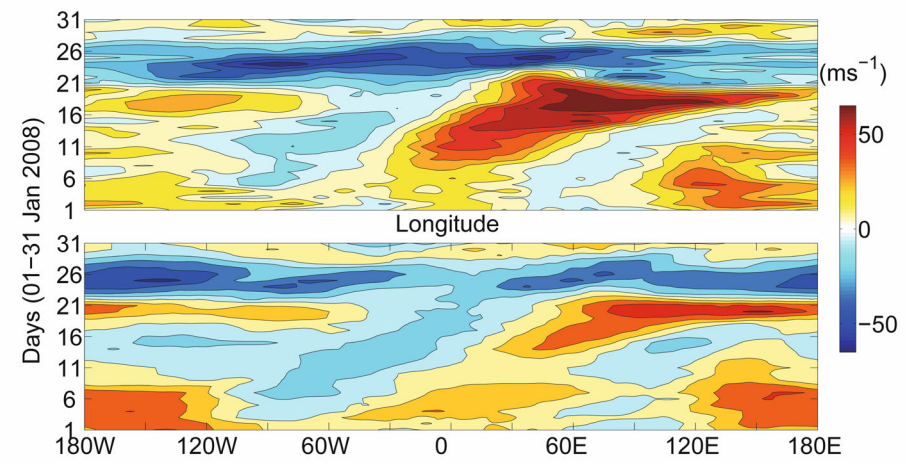

Fig. 1. Longitude–time section of reflective index. The differences between zonal wind at 2 hPa and 10 hPa, averaged over 58°–74°N (upper panel) and between 10 hPa and 50 hPa, averaged over the same grid (bottom panel), are shown. Negative and positive index values indicate reflective and nonreflective basic states, respectively.

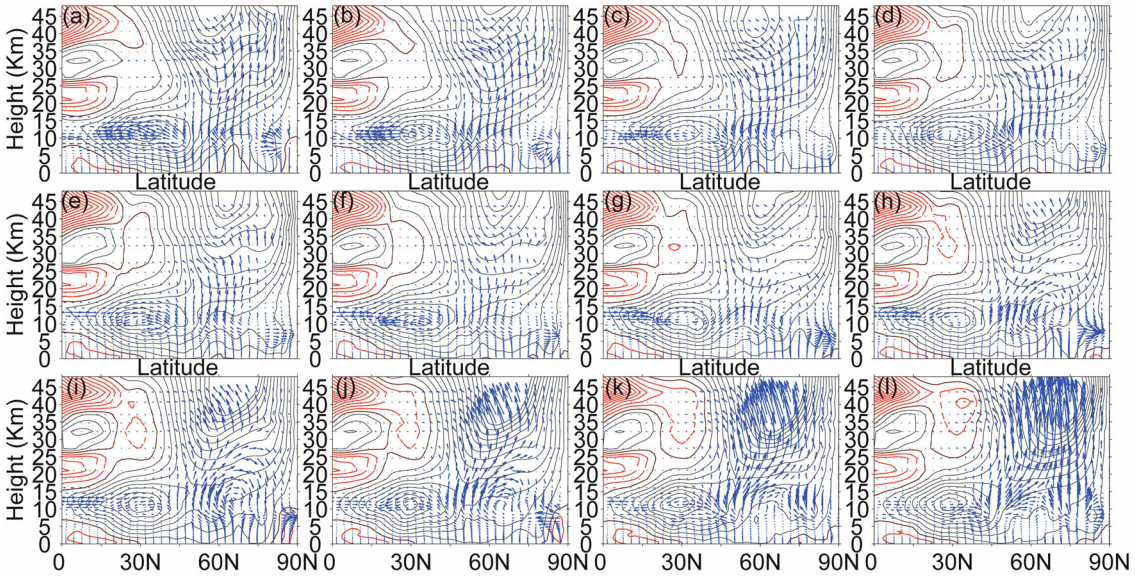

Fig. 2. Latitude-height section of zonal mean EP flux vectors (blue arrows), zonal mean zonal wind (black lines for westerly and red for easterly) during 10–21 January 2008 ((a)–(l)). The color shading interval is 5 m s^{-1}. Arrows are scaled with an order of 10 (meridional) and 1 (vertical).

heat flux (Fig. 3) to understand the evolution of the event with better clarity. As is clear from Figs. 2a and 3a, i.e., for 10 January, two planetary waveguides exist: the high-latitude waveguide between 40° and 60°N points from the lower troposphere toward the high-latitude stratosphere; whereas, another one points toward the upper troposphere at low latitudes. The features are consistent with those of Huang and Gambo (1982). On the other hand, the westerly wind over the midlatitudes provides a favorable background for the planetary waves to propagate upward (Dickinson, 1968) and the occurrence of the wave evanescent region above the subtropical tropopause (Hu and Tung, 2002) becomes more and more prominent due to the gradual descent of the zero wind contour from 40 km to 27 km as a function of time. Hence, our analysis is able to cover all the individual findings that were made by previous authors. From 11 January onwards, a gradual weakening and strengthening in the upward and downward component, respectively, of the high-latitude waveguide until 16 January can be noticed from Figs. 2b (3b)–2g (3g). Although the overturning in the high latitudes waveguide continues until 19 January, from 16 January onward the upward propagation of the planetary waves is restored again in response to the topographic forcing around 40°–45°N. The reflection ceases completely by 19 January and the entire high latitudes is dominated by the upward flux, which may be a precursor for the major sudden stratospheric warming event in the late January. The low-latitude waveguide behaves in a more or less similar fashion during the entire period of analysis.

3.2. *Wave propagation in the three-dimensional plane*

The above is the usual view of the two-dimensional propagation of planetary waves, but the planetary waves can also propagate zonally (Hayashi, 1981). Hence, the zonal mean may not provide a true impression of planetary wave propagation, especially when the basic state is partially reflective. To investigate the planetary wave activity, three-dimensional Plumb flux was calculated from Eq. (4) (Plumb, 1985). As is clear from the above discussion, the reflection phenomena are more likely to have occurred from 10 to 19 January, and hence we have plotted the vertical component of the Plumb flux at 200 hPa, averaged over the period (Fig. 4) mentioned above. It can be seen from Fig. 4 that the upward and downward propagation occurs in different geographic locations. A strong upward propagation of Plumb flux occurs over Baffin Island and the coast of Labrador and is reflected back to Central Eurasia (West Siberia) and parts of China. The zonal variation of Uri as a function of time is overplotted on Fig. 4. The upward and downward wave fluxes are confined to the west and east of the reflecting sectors (i.e., negative/zero index), respectively, indicating the role of the stratospheric polar jet to guide the tropospheric planetary wave pattern preferentially downward, eastward and slightly equatorward of the source region. Apart from this, the descending branch stretches meridionally until 25°N and hence the Plumb flux averaged over 30°–80°N are depicted in Figs. 5–8 together with the eddy geopotential height field, temperature and meridional wind anomaly from 10–21 January. The temperature and the meridional wind anomalies were calculated as the deviation from the datewise climatological mean values.

Figures 5, 6, 7 and 8 correspond to 10, 13, 16 and 19 January, respectively, and each one includes four panels, i.e., (a), (b), (c) and (d). Panel (a) depicts the eddy geopotential height (contours) overplotted with a longitude–height section of Plumb fluxes (arrows), averaged over 30°–80°N to illustrate

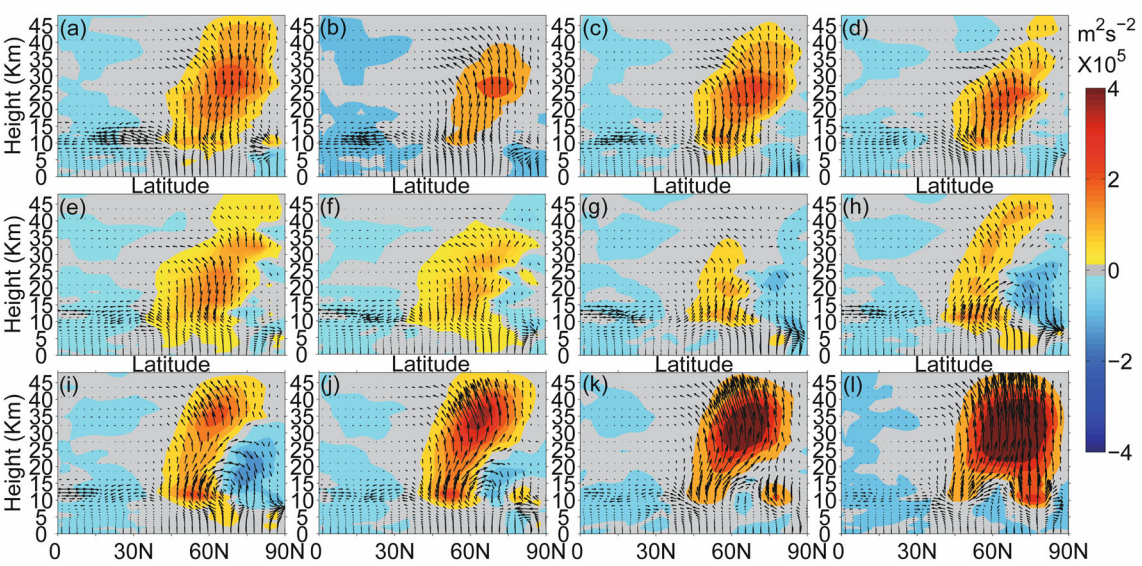

Fig. 3. Latitude–height section of zonal mean EP flux vectors (black arrows), zonal mean heat flux/vertical component of EP flux ($\times 10^5$ m^2 s^{-2}, color shading) during 10-21 January 2008 [(a)-(l)]. The positive and negative fluxes indicate the upward and downward wave propagation. Arrows are scaled with an order of 10 (meridional) and 1 (vertical).

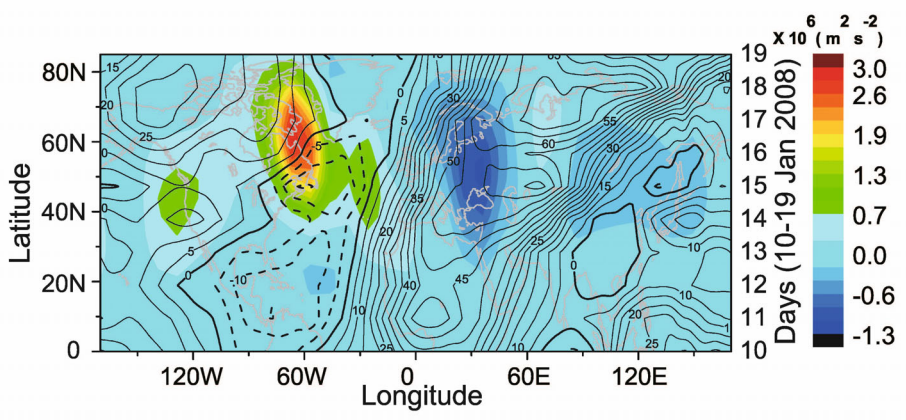

Fig. 4. Longitude–latitude section (bottom–left axis) of the vertical component of Plumb wave activity flux ($\times 10^6$ m^2 s^{-2}, color shading) at 200 hPa, averaged during 10–19 January 2008. The longitude–time section of reflective index ($U_{2\text{hpa}} - U_{10\text{hpa}}$) during 10–19 January is overplotted in the bottom-right axis (color-shaded with intervals of 5 m s^{-1}).

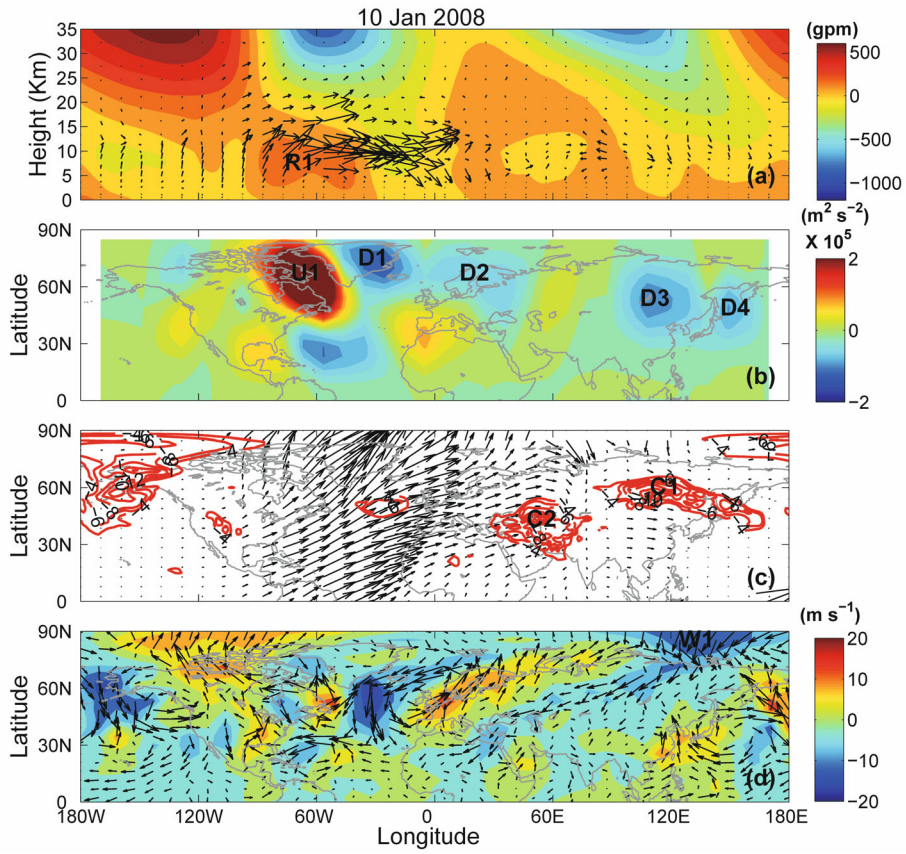

Fig. 5. (a) Longitude–height section of Plumb wave activity eddy flux (arrows), overplotted with eddy geopotential height (gpm, color shading), averaged over 30°–80°N; arrows are scaled with an order of 10^{-1} (zonal) and 10^{-7} (vertical). (b) Longitude–latitude section of Plumb vertical wave activity flux at 200 hPa ($\times 10^5$ m^2 s^{-2}, color shading). (c) Longitude–latitude section of Plumb wave activity flux (arrows) at 400 hPa and negative temperature anomalies (red color shading) at 850 hPa; arrows are scaled with an order of 1; color-shaded interval is 2°K. (d) Longitude–latitude section of meridional wind anomaly (m s^{-1}, color shading) at 850 hPa, overplotted with wind vectors at 850 hPa; arrows are scaled with 1 m s^{-1}. All the plots correspond to 10 January 2008.

the tropospheric aspect of the variation. Panel (b) represents the vertical component of Plumb wave activity flux (contours) at 200 hPa. Panel (c) includes the longitude–latitude section of Plumb flux (arrows) at 400 hPa and temperature anomaly at 850 hPa (negative temperature only; red contour lines), while the map of the meridional wind anomaly at 850 hPa (contours) overplotted with wind vectors (arrows) are shown in panel (d) to inspect the advection of cold northerly wind in response to the enhanced wave activity near the surface. Although we analyzed and discussed the daily variation (10–21 January) of all the parameters mentioned above, only the plots corresponding to 10, 13, 16 and 19 January are included in the paper for brevity.

In the mid troposphere, a ridge is located at around 60°W (hereafter R1) on 10 January 2008 (Fig. 5a). The R1 has shifted westward with increasing altitude, and at 10 hPa it is found at around 140°W. The westward tilt can be interpreted as an upward propagation of the Rossby waves (Kodera et al., 2008) over Baffin Island and the coast of Labrador (hereafter U1; Fig. 5b). U1 propagates upward and eastward in the upper troposphere and lower stratosphere (UTLS) and downward over Greenland (hereafter D1), Europe (hereafter D2), albeit weakly, central Russia (hereafter D3), and (again weakly) the Sea of Okhotsk (hereafter D4). In Fig. 5c the corresponding horizontal propagation patterns are consistent with the wave packets emanating from the Labrador coast and propagating from the North Atlantic to Eurasia. The increase of the wave activity in the lower troposphere due to reflection triggers thermal advection near the surface, and the facts are consistent with the southwestward excursion of cold polar air from Siberia (Fig. 5d), which might have contributed to the cold temperature anomaly over a wide region of Central Russia to the Sea of Okhotsk and northeastern parts of the Arabian Desert (Fig. 5c). On 11 and 12 January, R1 becomes more prominent and most of the wave fluxes propagate farther eastward, which in turn intensify the downward fluxes over the west coast of Europe and D2. On the other hand, D3 shifts a little westward and finally vanishes on 12 January, whereas wave packets (although weak) from the Canadian Tundra region and east coast of Greenland start to propagate upward, then intensify on 12 January, and finally merge with U1 on 13 January (hereafter MU1) (Fig. 6b). On 12 January the bridge between U1 and D2 develops clearly and R1 propagates rather horizontally eastward to $\sim 10°$E on 13 January (Fig. 6a), to $\sim 30°$E on 14 January, then attains its maximum when it reaches $\sim 50°$E on 16 January (Fig. 7a), and finally 120°E on 19 January (Fig. 8a) before disappearing by the end of the event. As a consequence, D2 and the sinks over Europe and the Mediterranean Sea develop extraordinarily on 13 January (Fig. 6b), culminating in a single dominant sink over the West Eurasian continent (hereafter MD1) on 14 January; whereas the sink over the east coast of Eurasia seems to freshly develop (hereafter D5). On 15 January, MD1 and D5 intensify further as R1 reaches $\sim 40°$E and wave pack-

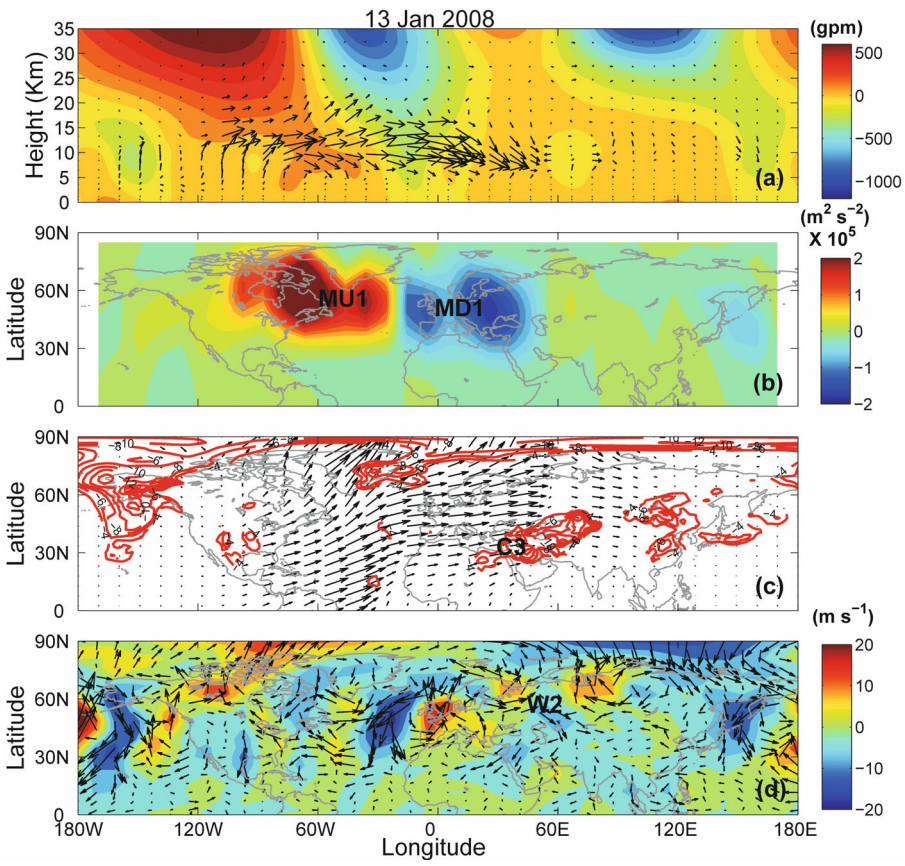

Fig. 6. The same as Fig. 5, but for 13 January 2008.

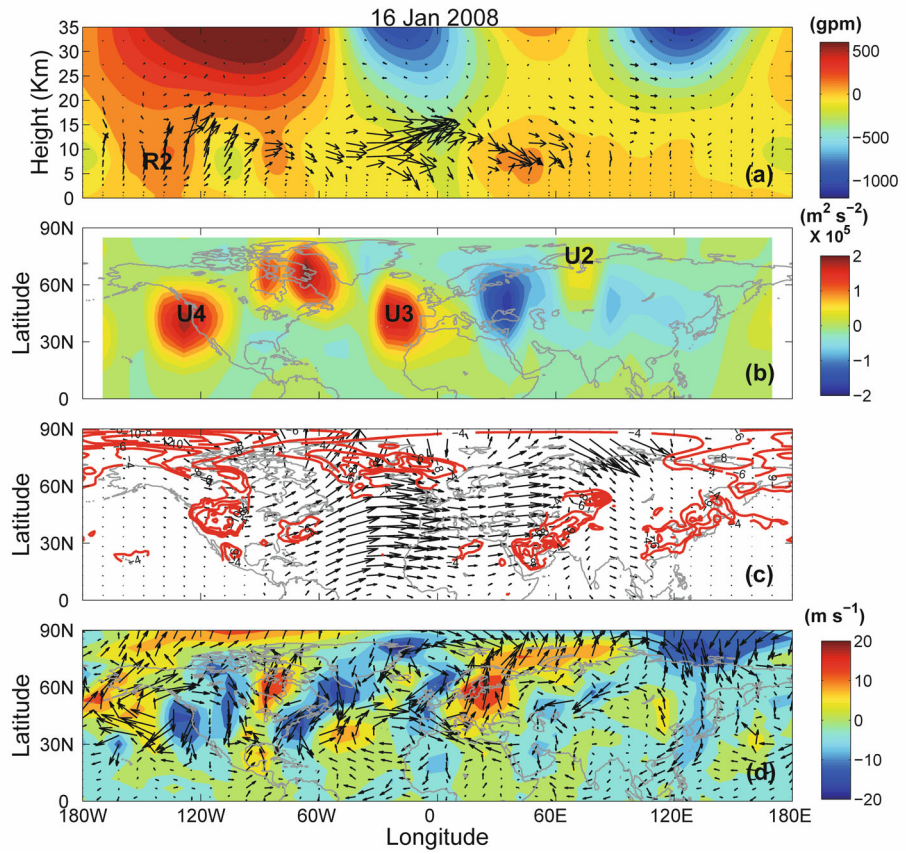

Fig. 7. The same as Fig. 5, but for 16 January 2008.

ets begin to propagate eastward from the Siberian Tundra region on 16 January (hereafter U2) (Fig. 7b). On 15 January MU1 stretches over the North Atlantic Ocean to the northwestern part of the Sahara Desert and finally separates out of MU1 (hereafter U3) until it fades away on 21 January. Whereas, the ridge at around $\sim 150°$W (hereafter R2) develops in response to the upward propagating fluxes over the Gulf of Alaska (hereafter U4) (Fig. 7b), and propagates farther eastward to 0° on 18 January and to $\sim 50°$E on 19 January (Fig. 8a). As a consequence, by 20 January, U4, U3 and U2 seem to extend over the Canadian Tundra to Hudson Bay, northern parts of the Sahara Desert and the Sea of Okhotsk, respectively, whereas MD1 and D5 shift a little eastward and westward to Central Eurasia (West Siberia) and Northwest China, respectively, on 17 January, until they disappear on 19 January (Fig. 8b). Hence, we can summarize from the above discussion that the ridge over 60°W (R1) propagated eastward to around 50°E, and finally to 120°E, in response to the waves propagating upward from the coast of Labrador/Baffin Island, and reflected back to Central Eurasia and central parts of China forming bridges between the two hemispheres due to the reflective stratospheric background state.

3.3. *Cold weather in relation with thermal advection, and blocking phenomena*

As mentioned, on 10 January the descending branch of the planetary waves over central Russia, i.e., D3 and D4 might have triggered the advection of cold polar air from Siberia (hereafter W1) (Fig. 5d) and contributed to the cold anomaly (as low as $-12°$C) over Central Russia to the Sea of Okhotsk (hereafter C1) and northeastern parts of the Arabian Desert (hereafter C2) (Fig. 5c). The eastward and equatorward propagation of C2 (Fig. 6c) is induced by anomalous development of northwesterly wind over the Caspian Sea (hereafter W2) (Fig. 6d), which is consistent with the gradual intensification of the descending branch of planetary waves over Europe (D2) on 13 January (Fig. 6b). As MD1 gradually develops, wind anomalies from the northern part of the boreal forest regions boost W2 on 14 January to advect C2 rather meridionally over the central part of the Arabian Desert; whereas the combined effect of D3, D4 and D5 initiate a branch of W1 to extend C1 over the eastern part of China on 16 January (Fig. 7c). Both C1 and C2 then propagate zonally eastward and C2 persists extraordinarily until 21 January over a wide area stretching from the Thar Desert to the South-central China (Fig. 8c), and seems to be responsible for the extreme cold weather in January 2008. However, the branch of anomalous northeasterly wind from Siberia (Fig. 5d) over the Arabian Desert induces a branch of C2 (hereafter C3) to propagate farther westward toward the Sahara Desert on 13 January (Fig. 6c), which finally intensifies to spread over the central part of the desert by 21 January. We further discuss the possible mechanisms in the following section.

It is well known that the possible mechanisms for the ad-

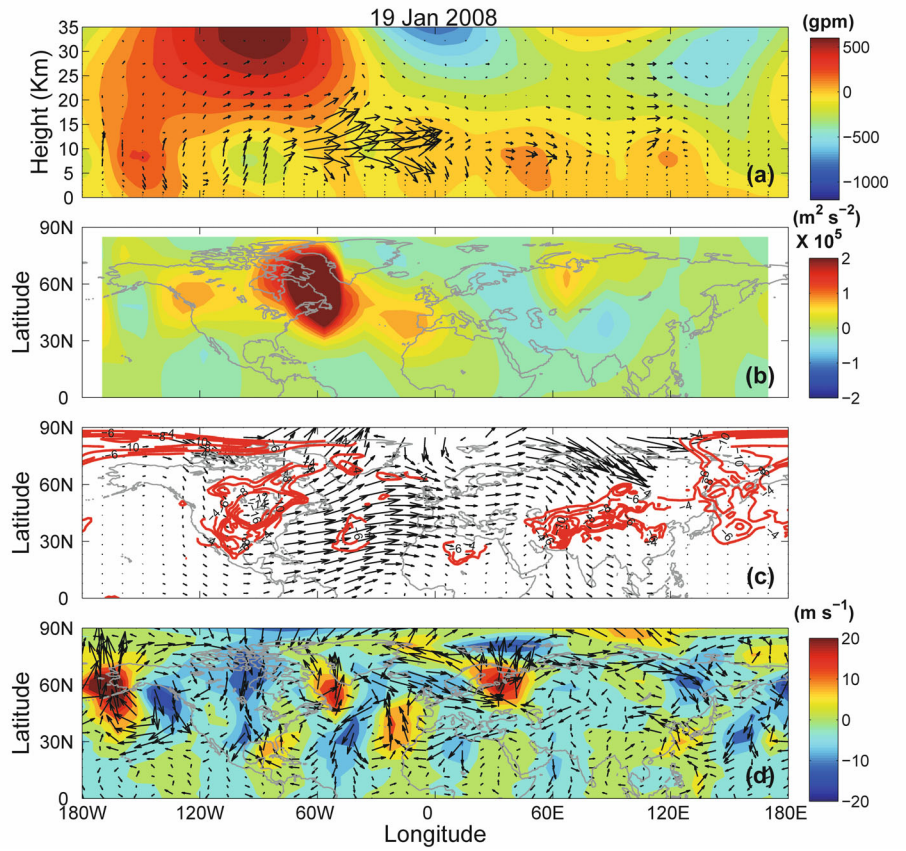

Fig. 8. The same as Fig. 5, but for 19 January 2008.

vection of cold polar air to low latitudes are the reflection of planetary waves, which may trigger thermal advection near the surface and bring an extreme cold anomaly to the subtropics/tropics, and the horizontal propagation of planetary waves or the development of an anomalous blocking high at 500 hPa, which might bring cold air in the downstream of the wave. In the present case study, it appears that planetary wave reflection might have played some role in triggering the advection during January 2008, but we cannot exclude the role from other factors such as a strong persistent southwesterly flow, a deep inversion layer in the lower troposphere, or persistent snow processes by a positive feedback process (Zhou et al., 2009). Since a blocking high occurred for extraordinary persistence of the cold temperature anomaly during that period, we calculated the blocking index using Eqs. 5 (a)–(b). To understand the time evolution of wave reflection in relation to the occurrence of cold temperature, we plotted (Fig. 9) the longitude–time section of the vertical component of Plumb wave activity flux and vectors at 200 hPa, averaged over 30°–80°N. Besides, we also plotted the longitude–time section of thermal advection, which we calculated using Eq. (6) and the temperature anomaly at 850 hPa, averaged over 20°–40°N (Figs. 10a and b, respectively). Figures 9 and 10 are overplotted with the longitude–time section of the blocking index at 500 hPa, and the bold contour lines indicate the blocked longitudes.

It can be seen that the ascending and descending branches are active around 30°–60° W and 30°–50°E, and 90°–120°E and 150°E, respectively, which is consistent with the source over the Baffin Island/Labrador coast and sinks over Europe, China/Central Russia and the Sea of Okhotsk, as discussed in section 3.2. We can clearly identify the strong reflection events in Fig. 9 during the first week of January and from 10–19 January. During the first event, the descending branches over 30°–50°E and 90°–120°E are strong enough and are accompanied by the simultaneous occurrence of a blocking high over the Euro-Atlantic region, stretching from 1–9 January. The geographical location and the temporal evolution of the cold advection (Fig. 10a) and hence the occurrence of the cold temperature anomaly (0°–80°E) coincides nicely with the former case (first week of January), but in the upstream position of the blocked longitudes. Hence, we can conclude that, for this particular event, thermal advection played the key role to drive the cold polar air to the subtropics. However, the occurrence of another cold event further east of the downstream of the blocked longitudes might have occurred due to the combined influence of thermal advection and an anomalous blocking high, but this needs further investigation and is out of scope for the present paper because it primarily deals with the extreme event that occurred in the late second and third week of January, which incurred a huge loss of property in China and some other Asian countries.

During the second event, i.e., 10 January onwards, reflection occurs at 30°–50°E; and finally, by 13 January, it ex-

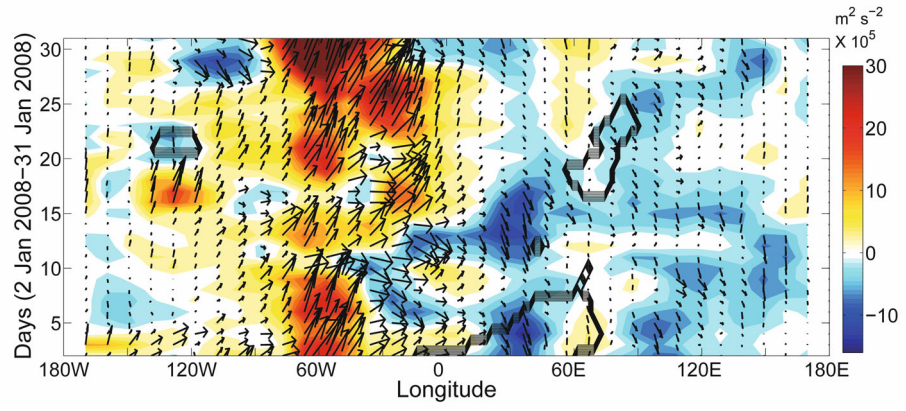

Fig. 9. Longitude–time section of the vertical component of Plumb wave activity flux (color shading) at 200 hPa, the zonal and vertical component of Plumb wave activity flux (arrows) at 200 hPa, averaged over 30°–80°N, and the 3-day running mean blocking index (bold color shading) at 500 hPa for January 2008. The arrows are scaled with an order of 1 (zonal) and 10^{-6} (vertical).

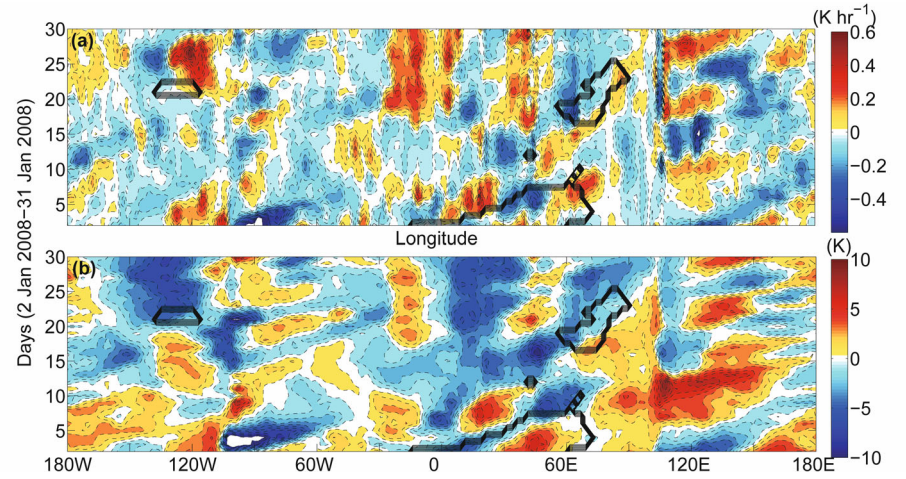

Fig. 10. Longitude–time section of thermal advection in K h^{-1} (a) and temperature anomaly in K (b) at 850 hPa, averaged over 20°–40°N, overplotted with the 3-day running mean blocking index at 500 hPa.

tends to 90°–120°E and 150°E (Fig. 9). As a consequence, advection of cold air from polar latitudes (Fig. 10a) substantially decreases the temperature to a minimum of −12°C over a wide region of Eurasia and parts of China. It can be seen that the blocks in the Euro-Atlantic region disappear by 10 January, reappear again on 16 January over the Urals–Siberia region, and persist until 26 January, but a gradual eastward tilt in the blocking pattern can be observed as a function of time. Zhou et al. (2009) reported the occurrence of snowstorm events, extreme low temperatures and freezing rain over southern China during 10–15 January, 18–22 January, 25–28 January, and 31 January to 2 February. Among these four events, the first two were more disastrous, not only in terms of intensity but also due to their extraordinary persistence. The snow cover over China increased significantly on 12 January and gradually attained its maximum by 21 January, which is consistent with our analysis, and the combined influence of wave reflection and the blocking high seem to have played the key role in at least the first two events. In the absence of blocking, planetary wave reflection is solely responsible for initiating the cold event over the Arabian Plateau (C1) and parts of China (C2) during 10–15 January (Fig. 9), whereas the extraordinary persistence of the event might have a close relationship with the occurrence of a strong blocking high from 16 January, as well as with the reflection phenomena. To further confirm our arguments, let us refer back to Fig. 5c where the wave vectors are preferentially horizontal from the North Atlantic to Central Eurasia during 10–15 January (e.g., Fig. 6c, 13 January) in response to the reflection phenomena, and the cold anomalies seem to propagate rather equatorward over the Arabian Plateau and parts of China. From 16 January onwards, R1 and U3 propagate farther eastward (Figs. 7a and 7b) and the horizontal wave fluxes over Siberia start to propagate eastward and equator-

ward (Fig. 7c). This triggers the anomalous northerly wind, which appears as a narrow tail from the Siberian Tundra region to the South China Sea (Figure 7 (d)), bringing cold anomalies from that region to the downstream of the wave (Figure 7c) and ultimately merges with C1. It then intensifies and propagates farther eastward over the North Pacific Ocean, whereas C2 extends over a wide area stretching from the Thar Desert to southern and central parts of China by 21 January. This eastward shift in the cold advection (Fig. 10a) and hence the cold temperature anomaly (Fig. 10 b) pattern for C1 and C2 are consistent with the eastward shift in the blocking pattern and R1, respectively; whereas by the end of January, C3 intensifies further and the wide region of the Sahara Desert experiences extreme cold weather. Thus, the cold anomalies over Asia during January 2008 were brought by the cumulative effects of planetary wave reflection and the occurrence of a strong blocking high over the Urals–Siberia region. In this context, it is worth mentioning that wave reflection and blocking contributed independently to this cold event, but in a separate study preliminary analysis indicates that wave reflection had a significant effect on the blocking around the Urals–Siberia region. More work is needed to clarify the conditions under which wave reflection contributed to the occurrence of the blocking high.

4. Summary and discussions

In the present paper, we have mainly discussed the occurrence of extreme cold events over the Asian subcontinent during 10–21 January 2008 with respect to planetary wave reflection from the stratosphere. As is clear from the daily march of EP flux vectors and heat flux, from 11 January onwards, a gradual weakening and strengthening in the upward and downward component, respectively, of the high-latitude waveguide took place. This can be seen until 16 January, and the overturning/reflection in the high-latitude waveguide continued until 19 January. However, zonal mean propagation may not be a true diagnostic for planetary wave propagation, especially when the basic state is partially reflective. Hence, we also plotted the Plumb three-dimensional wave activity fluxes and found that wave vectors propagated upward and downward from the Labrador/Baffin Island coast, Central Eurasia, and parts of China. These features are consistent with the eastward propagation of the ridge from 60°W to 40°E on 15, and finally to 120°E on 19 January, as well as with the southeastward propagation of the trough from Greenland stretching over a wide area from the Sahara Desert to the Tibetan Plateau on 15 January. The trough propagated farther eastward in response to the upward propagating fluxes from the Gulf of Alaska on 16 January.

We have also shown that, during the second 10 days of January 2008, along with other factors the combined influence of planetary wave reflection and the occurrence of a blocking high over the Urals–Siberia region might have played some role in the persistent cold weather over the Arabian Plateau and South-central China. Reflection of the WN1 pattern might have triggered thermal advection near the surface and brought extreme cold anomalies from the northern part of the boreal forest regions and Siberia, which seems to have played some role in the occurrence of the extreme snow event during 10–15 January. Whereas, the extraordinary persistence of the event might have occurred due to the anomalous blocking high over the Urals–Siberia region from 16 January, which would have brought more cold air from Siberia to the subtropics/tropics. Hence, we can conclude that planetary WN1 reflection during January 2008 played some role in influencing the tropospheric weather over parts of Asia.

Acknowledgements. This work was supported jointly by the National Basic Research Program of China (Grant No. 2010CB 428603), the National Natural Science Foundation of China (Grants Nos. 41250110073, 41350110331 and 41025017), the Chinese Academy of Sciences fellowship for young international scientists (Grant No. 2011Y2ZZB05), and a China postdoctoral science foundation grant (Grant No. 2013M541010).

REFERENCES

Andrews, D. G., J. R. Holton, and C. B. Leovy, 1987: *Middle Atmosphere Dynamics*. Academic Press Inc., 489 pp.

Baldwin, M. P., and T. J. Dunkerton, 1999: Propagation of the Arctic Oscillation from the stratosphere to the troposphere. *J. Geophys. Res.*, **104**, 30 937–30 946.

Baldwin, M. P., and T. J. Dunkerton, 2001: Stratospheric harbingers of anomalous weather regimes. *Science*, **294**, 581–584.

Barriopedro, D., R. C. G. Herrera, A. R. Lupo, E. Hernández, 2006: A climatology of Northern Hemisphere Blocking. *J. Climate*, **19**, 1042–1063.

Chen, W., and R. Huang, 2002: The propagation and transport effect of planetary waves in the Northern Hemisphere winter. *Adv. Atmos. Sci.*, **19**, 1113–1126.

Chen, W., and T. Li, 2007: Modulation of northern hemisphere wintertime stationary planetary wave activity: East Asian climate relationships by the Quasi-Biennial Oscillation. *J. Geophys. Res.*, **112**, D20120, doi: 10.1029/2007JD008611.

Chen, W., and K. Wei, 2009: Anomalous propagation of the quasi-stationary planetary waves in the atmosphere and its roles in the impact of the stratosphere on the East Asian winter climate. *Advances in Earth Science*, **24**, 272–285. (in Chinese)

Chen, W., H. F. Graf, and M. Takahashi, 2002: Observed interannual oscillations of planetary wave forcing in the Northern Hemisphere winter. *Geophys. Res. Lett.*, **29**(22), 2073, doi: 10.1029/2002GL016062.

Chen, W., K. Wei, L. Wang, and Q. Zhou, 2013: Climate variability and mechanisms of the East Asian winter monsoon and the impact from the stratosphere. *Chinese Journal of Atmospheric Sciences*, **37**(2), 425–438, doi: 10.3878/j.issn.1006-9895.2012.12309. (in Chinese)

Chen, Y. J., R. J. Zhou, S. M. Deng, M. J. Yi, and Y. Liu, 2009: Relationship between stratospheric circulation anomalies and extended snow storm. *Journal of University of Science and Technology of China*, **39**(1), 15–22. (in Chinese)

Christiansen, B., 2000: A model study of the dynamical connection between the Arctic Oscillation and stratospheric vacillations. *J. Geophys. Res.*, **105**, 29 461–29 474.

Christiansen, B., 2001: Downward propagation of zonal mean zonal wind anomalies from the stratosphere to the troposphere: Model and reanalysis. *J. Geophys. Res.*, **106**, 27 307–27 322.

Coughlin, K., and K. K. Tung, 2005: Tropospheric wave response to decelerated stratosphere seen as downward propagation in northern annular mode. *J. Geophys. Res.*, **110**, D01103, doi: 10.1029/2004JD004661.

Dee, D. P., and Coauthors, 2011: The ERA-Interim reanalysis: configuration and performance of the data assimilation system. *Quart. J. Roy. Meteor. Soc.*, **137**, 553–597.

Deng, S. M., Y. J. Chen, T. Luo, Y. Bi, and H. F. Zhou, 2008: The possible influence of stratospheric sudden warming on East Asian weather. *Adv. Atmos. Sci*,, **25**(5), 841–846, doi: 10.1007/s00376-008-0841-7.

Dickinson, R. E., 1968: Planetary Rossby waves propagating vertically through weak westerly wind wave guides. *J. Atmos. Sci.*, **25**, 984–1002.

Geller, M. A., and J. C. Alpert, 1980: Planetary wave coupling between the troposphere and the middle atmosphere as a possible sun-weather mechanism. *J. Atmos. Sci.*, **37**, 1197–1214.

Harada, Y., A. Goto, H. Hasegawa, N. Fujikawa, H. Naoe, and T. Hirooka, 2010: A major stratospheric sudden warming event in January 2009. *J. Atmos. Sci.*, **67**, 2052–2069.

Hayashi, Y., 1981: Vertical-zonal propagation of a stationary planetary wave packet. *J. Atmos. Sci.*, **38**, 1197–1214.

Hines, C. O., 1974: A possible mechanism for the production of sun-weather correlations. *J. Atmos. Sci.*, **31**, 589–591.

Holton, J. R., and C. Mass, 1976: Stratospheric vacillation cycles. *J. Atmos. Sci.*, **33**, 2218–2225.

Holton, J. R., 2004: *An Introduction to the Dynamic Meteorology*. 4th ed., Academic Press, 535 pp.

Hu, Y. Y., and K. K. Tung, 2002: Interannual and decadal variations of planetary wave activity, stratospheric cooling, and northern hemisphere annular mode. *J. Climate*, **15**, 1659–1673.

Huang, R. H., and K. Gambo, 1982: The response of a Hemispheric Multi-Level model atmosphere to forcing by topography and stationary Heat sources. *J. Meteor. Soc. Japan*, **60**, 78–92.

Hui, G., 2009: China's snow disaster in 2008, who is the principal player? *International Journal of Climatology*, **29**, 2191–2196, doi: 10.1002/joc.1859.

Kodera, K., and M. Chiba, 1995: Tropospheric circulation changes associated with stratospheric sudden warmings: A case study. *J. Geophys. Res.*, **100**, 11 055–11 068.

Kodera, K., K. Yamazaki, M. Chiba, and K. Shibata, 1990: Downward propagation of upper stratospheric mean zonal wind perturbation to thetroposphere. *Geophys. Res. Lett.*, **17**, 1263–1266.

Kodera, K., Y. Kuroda, and S. Pawson, 2000: Stratospheric sudden warmings and slowly propagating zonal-mean zonal wind anomalies. *J. Geophys. Res.*, **105**, 12 351–12 359.

Kodera, K., H. Mukougawa, and S. Itoh, 2008: Tropospheric impact of reflected planetary waves from the stratosphere. *Geophys. Res. Lett.*, **35**, L16806, doi: 10.1029/2008GL034575.

Kuroda, Y., and K. Kodera, 1999: Role of planetary waves in the stratosphere-troposphere coupled variability in the Northern Hemisphere winter. *Geophys. Res. Lett.*, **26**, 2375–2378.

Lan, X. Q., W. Chen, and L. Wang, 2012: Quasi-stationary planetary wave-mean flow interactions in the Northern Hemisphere stratosphere and their responses to ENSO events. *Sci. China (Earth Sci.)*, **55**, 405–417, doi: 10.1007/s11430-011-4345-4.

Li, Q., H. F. Graf, and X. F. Cui, 2011: The role of stationary and transient planetary waves in the maintenance of stratospheric polar vortex regimes in northern hemisphere winter. *Adv. Atmos. Sci.*, **28**(1), 187–194, doi: 10.1007/s00376-010-9163-7.

Li, L., C. Y. Li, J. Pan, and Y. K. Tan, 2012: On the differences and climate impacts of early and late stratospheric polar vortex breakup. *Adv. Atmos. Sci.*, **29**(5), 1119–1128, doi: 10.1007/s00376-012-1012-4.

Namias, J., and P. F. Clapp, 1951: Observational studies of general circulation patterns. *Compendium of Meteorology*, T. F. Malone, Ed., Amer. Meteor. Soc., 551–568.

Nath, D., S. Sridharan, S. Sathishkumar, S. Gurubaran, W. Chen, 2013: Lower stratospheric gravity wave activity over Gadanki (13.5°N, 79.2°E) during the stratospheric sudden warming of 2009: Link with potential vorticity intrusion near Indian sector. *Journal of Atmospheric and Solar- Terrestrial. Physics*, **94**, 54–64.

Perlwitz, J., and H. F. Graf, 2001: Troposphere-stratosphere dynamic coupling under strong and weak polar vortex conditions. *Geophys. Res. Lett.*, **28**, 271–274.

Perlwitz, J., and N. Harnik, 2003: Observational evidence of a stratospheric influence on the troposphere by planetary wave reflection. *J. Climate*, **16**, 3011–3026.

Perlwitz, J., and N. Harnik, 2004: Downward coupling between the stratosphere and troposphere: The relative roles of wave and zonal mean processes. *J. Climate*, **17**, 4902–4909.

Plumb, R. A., 1985: On the three-dimensional propagation of stationary waves. *J. Atmos. Sci.*, **42**, 217–229.

Tibaldi, S., and F. Molteni, 1990: On the operational predictability of blocking. *Tellus*, **42**, 343–365.

Treidl, R. A., E. C. Birch, and P. Sajecki, 1981: Blocking action in the Northern Hemisphere: A climatological study. *Atmos. -Ocean*, **19**, 1–23.

Uppala, S. M., D. Dee, S. Kobayashi, P. Berrisford, and A. Simmons, 2008: Towards a climate data-assimilation system: Status update of ERA-Interim. *ECMWF Newletter*, **115**, 12–18.

Wang, D. H., and Coauthors, 2009: A preliminary analysis of features and causes of the snow storm event over the southern China in January 2008. *Acta Meteorologica Sinica*, **23**, 374–386.

Wang, L., K. Kodera, and W. Chen, 2012: Observed triggering of tropical convection by a cold surge: Implications for MJO initiation. *Quart. J. Roy. Meteor. Soc.*, **138**, 1740–1750, doi: 10.1002/qj.1905.

Wen, M., S. Yang, A. Kumar, and P. Q. Zhang, 2009: An analysis of the large-scale climate anomalies associated with the snowstorms affecting China in January 2008. *Mon. Wea. Rev.*, **137**, 1111–1130.

Zhou, W., J. C. L. Chan, W. Chen, J. Ling, J. G. Pinto, and Y. Shao, 2009: Synoptic-scale controls of persistent low temperature and icy weather over Southern China in January 2008. *Mon. Wea. Rev.*, **137**, 3978–3991.